John von Neumann Institute for Computing

Spectral Properties of Strongly Correlated Electron Phonon Systems

Gerald Schubert, Andreas Alvermann, Alexander Weiße,
Georg Hager, Gerhard Wellein, and Holger Fehske

published in

NIC Symposium 2006 ,
G. Münster, D. Wolf, M. Kremer (Editors),
John von Neumann Institute for Computing, Jülich,
NIC Series, Vol. **32**, ISBN 3-00-017351-X, pp. 201-210, 2006.

http://www.fz-juelich.de/nic-series/volume32

Spectral Properties of Strongly Correlated Electron Phonon Systems

Gerald Schubert[1], **Andreas Alvermann**[1], **Alexander Weiße**[1], **Georg Hager**[2], **Gerhard Wellein**[2], **and Holger Fehske**[1]

[1] Institut für Physik, Universität Greifswald
17487 Greifswald, Germany
E-mail: {*schubert, alvermann, weisse, fehske*}*@physik.uni-greifswald.de*

[2] Regionales Rechenzentrum Erlangen, Universität Erlangen
91058 Erlangen, Germany
E-mail: {*georg.hager, gerhard.wellein*}*@rrze.uni-erlangen.de*

1 Introduction

In the last few years solid state physics has increasingly benefited from scientific computing, and the importance of numerical techniques is likely to keep on growing quickly in this field. Because of the high complexity of solids, which are made up of a huge number of interacting electrons and nuclei, a full understanding of their properties cannot be developed using analytical methods only. Numerical simulations do not only provide quantitative results for the properties of specific materials but are also widely used to test the validity of theories and analytical approaches.

Unbiased numerical approaches, like exact diagonalisation (ED)[1], or the density matrix renormalisation group (DMRG)[2] are of particular importance for the investigation of low-energy and low-temperature electronic, optical, or magnetic properties of various novel materials, which cannot be understood within traditional many-particle theory. In such strongly correlated systems, the interactions between the constituents of the solid are so strong that they can no longer be considered separately and collective effects emerge. As a result, these systems may exhibit new and fascinating macroscopic properties. Quasi-one-dimensional (1d) electron-phonon (EP) systems like MX-chain compounds are prominent examples of electronic systems very different from traditional ones[3]. Their study is particularly rewarding for a number of reasons. First they exhibit a remarkably wide range of competing forces, which gives rise to a rich variety of different phases, characterised by symmetry-broken ground states and long-range orders. Second, 1d models allow us to investigate this complex interplay, which is important but poorly understood also in 2d and 3d highly-correlated electron systems, in a context more favourable to numerical simulations. Because the complexity of the systems leads to huge requirements of memory and CPU time, access to large computational resources is necessary.

2 Models

Experiments on a variety of novel materials, ranging from quasi-1d MX solids[3], organics[4] and quasi-2d high T_c cuprates[5] to 3d colossal-magnetoresistive manganites[6], provide clear evidence for the existence of polaronic carriers, i.e., quasi particles consisting of an electron

and a surrounding lattice distortion. This has motivated considerable theoretical efforts to archive a better understanding of strongly coupled EP systems in the framework of microscopic models.

To describe the interplay between electrons and the dynamics of the lattice, which is known to play a key role for instance in quasi-1d metals and charge-density-wave (CDW) systems, one of the simplest model is the Holstein-Hubbard model (HHM):

$$H = -t \sum_{\langle i,j\rangle\sigma} c^\dagger_{i\sigma} c_{j\sigma} - g\omega_0 \sum_{i\sigma} (b^\dagger_i + b_i) n_{i\sigma} + \omega_0 \sum_i b^\dagger_i b_i + U \sum_i n_{i\uparrow} n_{i\downarrow} \,. \qquad (1)$$

Here $c^\dagger_{i\sigma}$ ($c_{i\sigma}$) denote fermionic creation (annihilation) operators of electrons with spin $\sigma =\uparrow, \downarrow$ on site i of a 1d lattice with N sites, $n_{i\sigma} = c^\dagger_{i\sigma} c_{i\sigma}$, and $b^\dagger_i$ (b_i) are the corresponding bosonic operators for dispersionless optical phonons. The physics of the HHM is governed by three competing effects: The itinerancy of the electrons ($\propto t$), their on-site Coulomb repulsion ($\propto U$), and the local EP coupling ($\propto g$). Since the EP interaction is retarded, the phonon frequency (ω_0) defines a further relevant energy scale. Hence, besides the adiabaticity ratio (ω_0/t) we need two dimensionless coupling constants ($u = U/4t$ and $\lambda = 2\varepsilon_{\rm p}/2t$ or $g^2 = \varepsilon_{\rm p}/\omega_0$). In the single-electron case, where the spin degree of freedom and the Coulomb interaction are irrelevant, the Holstein model[7],

$$H = -t \sum_{\langle i,j\rangle} c^\dagger_i c_j - \sqrt{\varepsilon_p \omega_0} \sum_i (b^\dagger_i + b_i) n_i + \omega_0 \sum_i b^\dagger_i b_i \,, \qquad (2)$$

has been studied extensively as a paradigmatic model for polaron formation[8]. Here $\varepsilon_{\rm p}$ gives the polaron binding energy.

As yet, none of the various analytical treatments, based on weak- and strong-coupling adiabatic and anti-adiabatic perturbation expansions[9], are suited to investigate the physically most interesting polaron transition region. Here, the characteristic electronic and phononic energy scales are not well separated and non-adiabatic effects become increasingly important. This implies a breakdown of the standard Migdal approximation. Quasi-approximation-free numerical methods like quantum Monte Carlo (QMC)[10,11] or ED and DMRG can, in principle, bridge the gap between the weak- and strong-EP-coupling limits, and currently represent the most reliable tools to study polarons close to the cross-over regime[12].

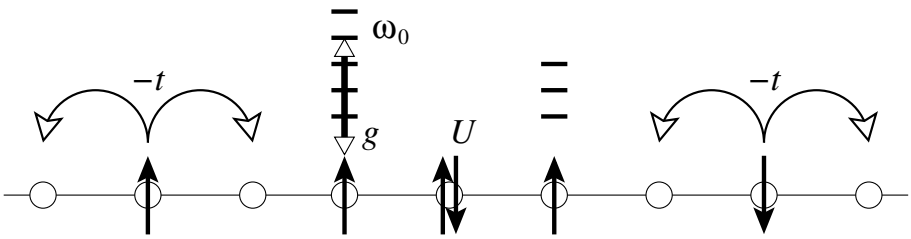

Figure 1. Schematic representation of the 1d Holstein-Hubbard model.

3 Implementation of Matrix Vector Multiplication (MVM)

The core operation of most ED and DMRG algorithms is a MVM. It is quite obvious, that our matrices are extremely sparse because the number of non-zero entries per row of our Hamilton matrix scales linearly with the number of electrons. Therefore a standard implementation of the MVM step uses a sparse storage format for the matrix, holding the non-zero elements only. Two data schemes are in wide use, the compressed row storage (CRS) and the jagged diagonal storage (JDS) format, where the latter one is the method of choice for vector computers. The typical storage requirement per non-zero entry is 12-16 Byte for both methods, i.e. for a matrix dimension of $\tilde{D} = 10^9$ about one TByte main memory is required to store only the matrix elements of the EP Hamiltonian. Both variants can be applied to any sparse matrix structure and the MVM step can be be done in parallel by using a parallel library such as PETSc (see `http://www-unix.mcs.anl.gov/petsc/petsc-as/`).

To extend our EP studies to even larger matrix sizes we store no longer the non-zero matrix elements but generate them in each MVM step. Of course, at that point standard libraries are no longer useful and a parallel code tailored to each specific class of Hamiltonians must be developed. For the Holstein-Hubbard EP model we have established a massively parallel program using the Message Passing Interface (MPI) standard. The minimal total memory requirement of this implementation is three vectors with Hilbert space dimension.

The parallelisation approach follows the inherent natural parallelism of the Hilbert space, which can be constructed as the tensorial product space of electrons and phonons $\{|\tilde{b}\rangle = |\tilde{e}\rangle \otimes |p\rangle\}$. Assuming, that the electronic dimension ($\tilde{D}_e$) is a multiple of the number of processors used (N_{cpu}) we can easily distribute the electronic basis states among these processors, i.e. processor $i (0 \leq i \leq N_{\mathrm{cpu}} - 1)$ is holding the basis states ($\tilde{e}_i = i\tilde{D}_e/N_{\mathrm{cpu}} + 1, \ldots, (i+1)D_e/N_{\mathrm{cpu}}$). As a consequence of this choice only the electronic hopping term generates inter-processor communication in the MVM while all other (diagonal electronic) contributions can be computed locally on each processor.

Furthermore, the communication pattern remains constant within a single run for all MVM steps and the message sizes (at least D_p words) are large enough to ignore the latency problems of modern interconnects. Using supercomputers with hundreds of processors and one TBytes of main memory, such as IBM p690 clusters or SGI Altix systems, we are able to run simulations up to a matrix dimension of 30×10^9.

4 Spectral Properties

4.1 Photoemission Spectra

Examining the dynamical properties of polarons, it is of particular interest whether a quasi-particle-like excitation exists in the spectrum. This is probed by direct (inverse) photoemission, where a bare electron is removed (added) from (to) the many-particle system containing N_e electrons. The intensities (transition amplitudes) of these processes are determined by the imaginary part of the retarded one-particle Green's functions,

$$G^{\pm}(k,\omega) = \langle\langle c_k^{\mp}; c_k^{\pm}\rangle\rangle_{\omega} = \lim_{\eta \to 0^+} \langle\psi_0| c_k^{\mp} \left[\omega + \mathrm{i}\eta - H\right]^{-1} c_k^{\pm} |\psi_0\rangle \,, \tag{3}$$

i.e., by the momentum resolved spectral functions

$$A^{\pm}(k,\omega) = -\frac{1}{\pi}\mathrm{Im}\, G^{\pm}(k,\omega) = \sum_m |\langle\psi_m^{\pm}|c_k^{\pm}|\psi_0\rangle|^2\, \delta[\omega \mp (E_m^{\pm} - E_0)] \qquad (4)$$

and $A(k,\omega) = A^+(k,\omega) + A^-(k,\omega)$, with $c_k^+ = c_k^\dagger$ and $c_k^- = c_k$. These functions test both the excitation energies $E_m^{\pm} - E_0$ and the overlap of the ground state $|\psi_0\rangle$ with the exact eigenstates $|\psi_m^{\pm}\rangle$ of a $(N_\mathrm{e} \pm 1)$-particle system. Hence, $G^+(k,\omega)$ $[G^-(k,\omega)]$ describes the propagation of an additional electron [a hole] with momentum k $[-k]$ and energy ω. The electron spectral function of the single-particle Holstein model corresponds to $N_\mathrm{e} = 0$, i.e., $A^-(k,\omega) \equiv 0$. $A(k,\omega)$ can be determined, e.g., by cluster perturbation theory (CPT)[13,12]: We first calculate the Green's function $G_{ij}^c(\omega)$ of a N_c-site cluster with open boundary conditions for $i,j = 1,\ldots,N_c$, and then recover the infinite lattice by pasting identical copies of this cluster along the edges, treating the inter-cluster hopping in first-order perturbation theory.

Figure 2 shows that at *weak coupling* (left panel), the electronic spectrum is nearly unaffected for energies below the phonon emission threshold. Hence, for the case considered here with ω_0 lying inside the bare electron bandwidth $4t$, the renormalised dispersion $E(k)$ follows the tight-binding cosine dispersion (lowered $\propto \varepsilon_p$) up to some k_X, where the dispersionless phonon intersects the bare electron band. For $k > k_X$, electron and phonon states "hybridise", and repel each other, leading to the well-known band-flattening phenomenon[14]. The high-energy incoherent part of the spectrum is broadened $\propto \varepsilon_p$, with the k-dependent maximum again following the bare cosine dispersion.

The inverse photoemission spectrum in the *strong-coupling case* is shown in the right panel of Fig. 2. First, we observe all signatures of the famous polaronic band-collapse, where a well-separated, narrow (i.e., strongly renormalised), coherent QP band is formed at $\omega \simeq -\varepsilon_p$. If we had calculated the polaronic instead of the electronic spectral function (4), nearly all spectral weight would reside in the coherent part, i.e., in the small-polaron band[15]. In contrast, the wave-vector renormalisation factor $Z(k)$ is extremely small and approaches the strong-coupling result $Z = \exp(-g^2)$ for $\lambda, g^2 \gg 1$. Note

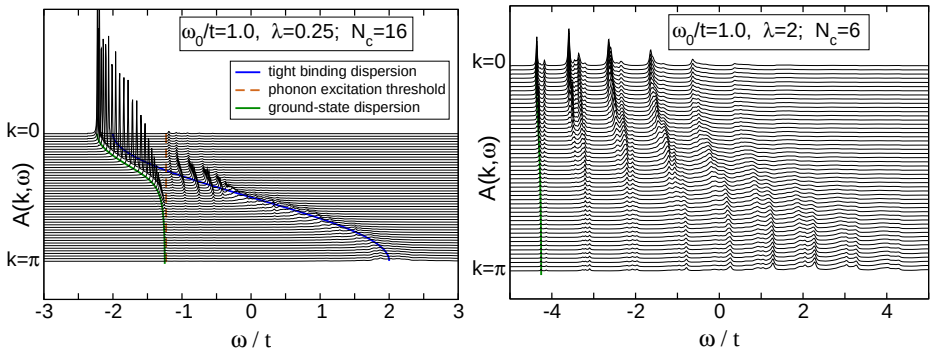

Figure 2. Spectral function of the 1d Holstein polaron calculated within CPT in the weak (left) and strong (right) non-adiabatic EP coupling regime. CPT is based on ED of a finite cluster with N_c sites and $M = 7$ ($\lambda = 0.25$) and $M = 25$ ($\lambda = 2$) phonon quanta.

that the inverse effective mass m^*/m_0 and $Z(k)$ differ if the self-energy is strongly k-dependent. This discrepancy has its maximum in the intermediate-coupling regime for 1D systems, but vanishes in the limit $\lambda \to \infty$ and, in any case, for $D = \infty$[16]. The incoherent part of the spectrum is split into several sub-bands separated in energy by ω_0, corresponding to excitations of an electron and one or more phonons (Fig. 2).

4.2 Optical Response

We apply the ED-KPM scheme outlined in[12,17,18] to calculate the optical absorption of the single-electron Holstein model. The results for the (regular) real part of the conductivity,

$$\mathrm{Re}\,\sigma(\omega) = \frac{\pi}{\omega N} \sum_{E_m > E_0} |\langle \psi_m | \hat{\jmath} | \psi_0 \rangle|^2 \, \delta[\omega - (E_m - E_0)] \tag{5}$$

(here $\hat{\jmath} = -\mathrm{i}et \sum_i (c_i^\dagger c_{i+1} - c_{i+1}^\dagger c_i)$ is the current operator), and possible deviations from established polaron theory are important for relating theory to experiment. For $T = 0$ the standard description of small polaron transport[19] yields (in leading order) the ac conductivity $\mathrm{Re}\,\sigma(\omega) = (\sigma_0/\omega\sqrt{\varepsilon_p \omega_0}) \exp\left[-(\omega - 2\varepsilon_p)^2/4\varepsilon_p\omega_0\right]$, which for sufficiently strong coupling predicts a weakly asymmetric Gaussian absorption peak centred at twice the polaron binding energy.

Figure 3 shows $\mathrm{Re}\,\sigma(\omega)$ when polaron formation sets in (left panel), and above the transition point (right panel). For $\lambda = 2$ and $\omega_0/t = 0.4$, i.e., at rather large EP coupling but not in the extreme small-polaron limit, we find a pronounced maximum in the low-temperature optical response, which, however, is located below $2\varepsilon_p$, the value for small polarons at $T = 0$. At the same time, the line-shape is more asymmetric than in small-polaron theory, with a weaker decay at the high-energy side, fitting even better to experiments on standard polaronic materials such as TiO_2[20]. At smaller couplings, significant deviations from a Gaussian-like absorption are found, i.e., polaron motion is not adequately described as hopping of a self-trapped carrier almost localised on a single site.

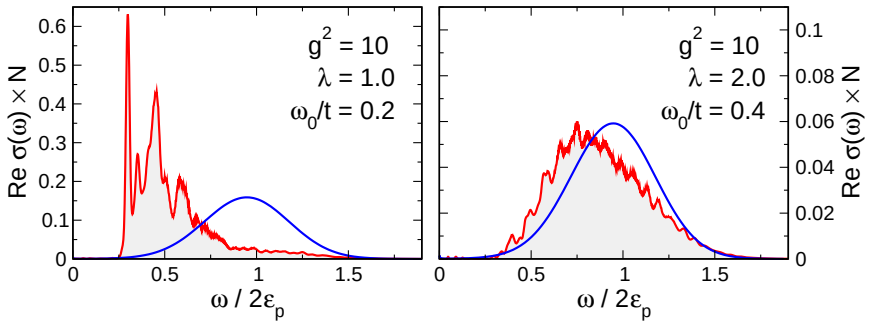

Figure 3. Optical conductivity (red, in units of $\pi e^2 t^2$) of the 1d Holstein model at $T = 0$ compared to the analytical small-polaron result (blue). ED data are for a system with six sites and 45 phonons; σ_0 is determined to give the same integrated spectral weight as $\mathrm{Re}\,\sigma(\omega > 0)$.

5 Quantum Phase Transitions in 1d Electron-Phonon Systems

Most notably quasi-1d materials are very susceptible to structural distortions driven by EP interaction. Probably the most famous one is the Peierls instability[21] of 1d metals: As the temperature is lowered the system creates a periodic variation in the carrier density by shifting the ions from their symmetric positions. For the half-filled band case this CDW is commensurate with the lattice, the unit cell doubles, and the system possesses a spontaneous broken-symmetry ground state. Since a static dimerisation of the lattice opens a gap at the Fermi surface the metal gives way to a Peierls insulator (PI) [see Fig. 4].

The on-site Coulomb interaction, on the other hand, tends to immobilise the charge carriers and establish a Mott insulating ground state. The Mott insulator (MI) exhibits strong spin density wave (SDW) correlations but has continuous symmetry and therefore shows no long-range order in 1d. Then, of course, the question arises, whether the PI and MI phases are separated by one (or more than one) quantum critical point(s) at $T = 0$, and if so, how the cross-over is modified by quantum phonon effects.

The challenge of understanding such quantum phase transitions has stimulated intense work on the Holstein Hubbard model. As yet there exist almost no exact (analytical) results for this model. At least at half-filling, however, it has become generally accepted that the interplay of charge, spin and lattice degrees of freedom gives rise to the phase diagram sketched in Fig. 5. This scenario is supported by dynamical mean field investigations of

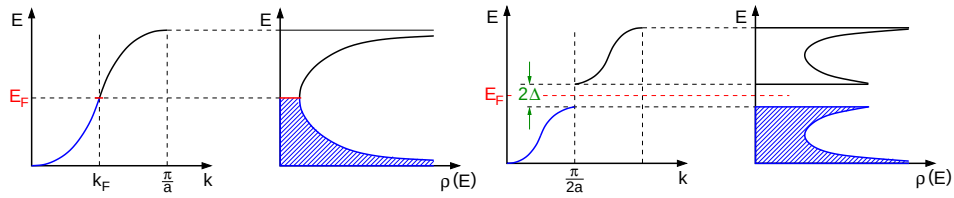

Figure 4. Peierls scenario: A gap 2Δ opens in the electronic band structure $E(k)$ [density of states $\rho(E)$] of an 1d metal if, as a result of the EP coupling, a static lattice distortion occurs, implicating a new lattice period $2a$ in real space.

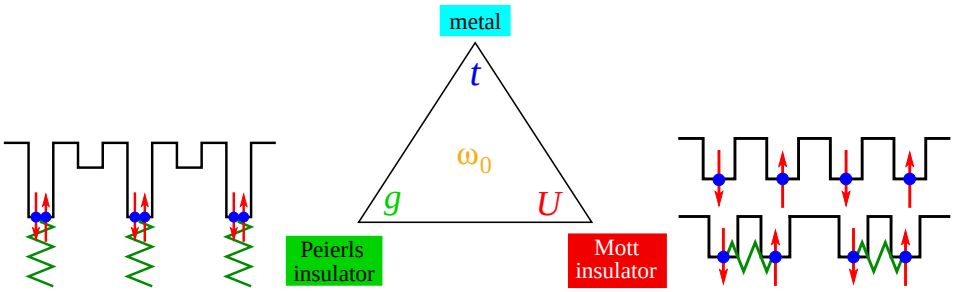

Figure 5. Schematic phase diagram of the 1d Holstein Hubbard model. At half-filling, Peierls (left) or Mott (right) insulating phases may be favoured over the metallic state. In the case of localised electrons interacting via antiferromagnetic exchange and magneto-elastic couplings even a spin-Peierls distorted state can emerge (right, lower panel).

the HHM, which become reliable at least in infinite spatial dimension[22].

Besides the properties of the ground state, the nature of the physical excitations is puzzling as well, especially in 1d. While one expects "normal" electron-hole pair excitations in the PI phase ($U = 0$), charge (spin) excitations are known to be massive (gapless) in the MI state of the Hubbard model ($\lambda = 0$). Thus, varying the control parameter u/λ, a cross-over from standard quasi-particle behaviour to spin-charge separation can be observed in the 1d HHM.

Since many-body gaps to excited states form the basis for making contact with experimentally measurable excitation gaps and can also be used to characterise different phases

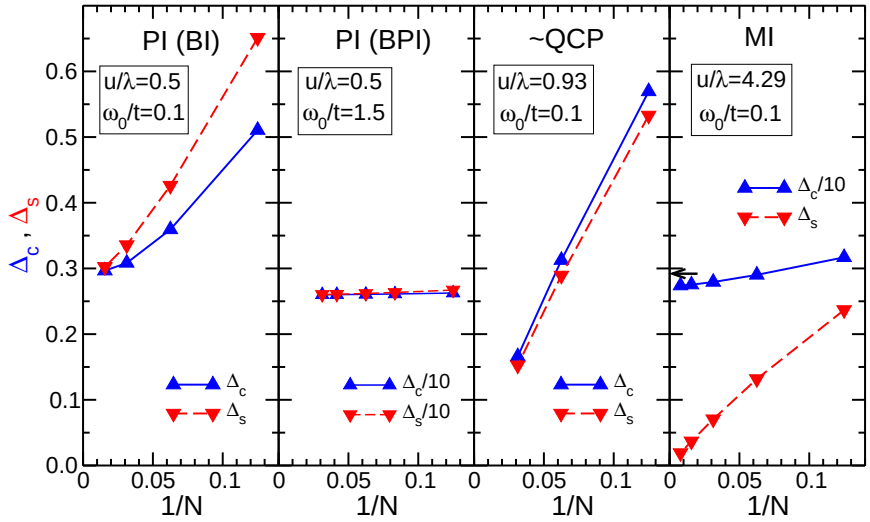

Figure 6. DMRG finite-size scaling of spin- and charge excitation gaps in the HHM at $\lambda = 0.35$ and $\omega_0/t = 0.1$). Open and filled symbols denote DMRG results for PBC and OPC boundary conditions, respectively. The accessible system sizes are smaller at larger λ/u, where an increasing number of (phononic) pseudo-sites is required to reach convergence with respect to the phonons. Stars represent the ED results for the eight-site system. The arrow marks the value of the optical gap $\Delta_{\rm opt}$ for the Bethe ansatz solvable 1d Hubbard model, which is given by $\Delta_{\rm opt}/4t = u - 1 + \ln(2)/2u$ in the limit of large $u > 1$[23].

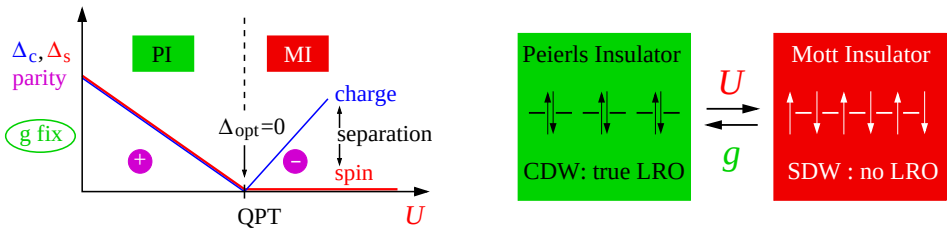

Figure 7. Sketch of the PI-MI quantum phase transition in the Holstein Hubbard model.

of the HHM, we have determine the charge and spin gaps,

$$\Delta_{\rm c} = E_0^+(1/2) + E_0^-(-1/2) - 2E_0(0) \tag{6}$$

$$\Delta_{\rm s} = E_0(1) - E_0(0)\,, \tag{7}$$

using DMRG, supplemented by a finite-size scaling. Here $E_0^{(\pm)}(S^z)$ is the ground-state energy of the HHM at half-filling (with $N_{\rm e} = N \pm 1$) particles in the sector with total spin-z component S^z.

Obviously, $\Delta_{\rm c}$ and $\Delta_{\rm s}$ are finite in the PI and converge to the same value for $N \to \infty$. Both gaps seem to vanish at the QCP of the HHM with finite-frequency phonons, but the finite-size scaling is extremely delicate in the critical region. In the MI we found a finite charge excitation gap, which in the limit $u/\lambda \gg 1$ scales to the optical gap of the Hubbard model, whereas the extrapolated spin gap remains zero. This can be taken as a clear indication for spin charge separation.

From our conductivity data for the half-filled band case (not shown) we found evidence for only one critical point separating Peierls and Mott insulating phases in the Holstein Hubbard model with dynamical phonons (by contrast in the adiabatic limit ($\omega_0 = 0$) two successive transitions have been detected for weak couplings u, $\lambda \ll 1$[24]). We have explicitly verified that the parity is $P = +1$ ($P = -1$) in the PI (MI) phase. The emerging physical picture can be summarised by the phase diagram shown in Fig. 7.

6 Summary

In this contribution, we have analysed the spectral properties of Holstein polarons as well as the transition from a Peierls- to Mott-insulator by means of quasi-exact numerical methods, such as Jacobi-Davidson based exact diagonalisation, kernel polynomial expansion techniques, density matrix renormalisation group and cluster perturbation theory, implemented on the NIC supercomputers. Our numerical approaches yield unbiased results in all parameter regimes, and are of particular value in the non-adiabatic intermediate-coupling regime, where perturbation theories and other analytical techniques fail.

Acknowledgements

We are grateful to A. R. Bishop, M. Hohenadler, D. Ihle, E. Jeckelmann and J. Loos for helpful discussions. Special thanks go to NIC Jülich for granting access to their supercomputer facilities.

References

1. J. Ranninger and U. Thibblin. *Phys. Rev. B*, 45:7730, 1992.
2. E. Jeckelmann and S. R. White. *Phys. Rev. Lett.*, 80:2661, 1998.
3. A. R. Bishop and B. I. Swanson. *Los Alamos Science*, 21:133, 1993.
4. I. H. Campbell and D. L. Smith. *Solid State Physics*, 55:1, 2001.
5. A. S. Alexandrov and N. F. Mott. *Polarons and Bipolarons*. World Scientific, Singapore, 1995.
6. G. Zhao, K. Conder, H. Keller, and K. A Müller. *Nature*, 381:676, 1996.
7. T. Holstein. *Ann. Phys. (N.Y.)*, 8:325, 1959.
8. H. Fehske, A. Alvermann, M. Hohenadler, and G. Wellein. *Proceedings of the "Enrico Fermi" Summer School, Course CLXI -"Polarons in Bulk Materials and Systems with Reduced Dimensionality"*, Varenna, 2005.
9. A. B. Migdal. *Sov. Phys. JETP*, 7:999, 1958.
10. H. De Raedt and A. Lagendijk. *Phys. Rev. B*, 27:6097, 1983.
11. M. Hohenadler, D. Neuber, W. von der Linden, G. Wellein, J. Loos, and H. Fehske. *Phys. Rev. B*, 71:245111, 2005.
12. E. Jeckelmann and H. Fehske. *Proceedings of the "Enrico Fermi" Summer School, Course CLXI -"Polarons in Bulk Materials and Systems with Reduced Dimensionality"*, Varenna, 2005.
13. D. Sénéchal, D. Perez, and M. Pioro-Ladrière. *Phys. Rev. Lett.*, 84:522–525, 2000.
14. G. Wellein and H. Fehske. *Phys. Rev. B*, 56:4513, 1997.
15. H. Fehske, J. Loos, and G. Wellein. *Z. Phys. B*, 104:619, 1997.
16. L.-C. Ku, S. A. Trugman, and J. Bonča. *Phys. Rev. B*, 65:174306, 2002.
17. A. Weiße, G. Wellein, A. Alvermann, and H. Fehske. preprint, 2005, `http://arXiv.org/abs/cond-mat/0504627`.
18. G. Schubert, G. Wellein, A. Weiße, A. Alvermann, and H. Fehske. *Phys. Rev. B*, 72:104304, 2005.
19. D. Emin. *Phys. Rev. B*, 48:13691, 1993.
20. E. K. Kudinov, D. N. Mirlin, and Y. A. Firsov. *Fiz. Tverd. Tela*, 11:2789, 1969.
21. R. Peierls. *Quantum theory of solids*. Oxford University Press, Oxford, 1955.
22. M. Capone and S. Ciuchi. *Phys. Rev. Lett.*, 91:186405, 1990.
23. A. A. Ovchinnikov. *Sov. Phys. JETP*, 30:1160, 1970.
24. H. Fehske, A. P. Kampf, M. Sekania, and G. Wellein. *Eur. Phys. J. B*, 31:11, 2003.